Spectral properties of entangled photon pairs generated via quasi-phased-matched spontaneous parametric down-conversion

Maopeng Xia (夏茂鹏), Jianjun Li (李健军), Youbo Hu (胡友勃), Wenyang Sheng (盛文阳), Dongyang Gao (高冬阳), Weiwei Pang (庞伟伟), and Xiaobing Zheng (郑小兵)*

Key Laboratory of Optical Calibration and Characterization, Chinese Academy of Sciences, Hefei 230031, China
**Corresponding author: xbzheng@aiofm.ac.cn*

Received June 30, 2015; accepted September 10, 2015; posted online October 16, 2015

The spectral properties of entangled photon pairs generated via quasi-phased matching in spontaneous parametric down-conversion are proposed and demonstrated experimentally. A general mathematical model for evaluating the spectral properties is developed to obtain the spectrum shape and range of down-converted photons. The model takes into account the effects of phase mismatching due to non-ideal pumping and the relationship between crystal periodic modulation function and the incidence angle of the pump beam. The spectrum curve shape is determined by the discrete Fourier transform of a Gaussian pump beam and the integration of parametric down-conversion generated by an individual plane wave. An experiment is carried out with a PPLN non-linear crystal and dispersing optics, which shows a good consistency in their spectral ranges and shapes with our model predictions within the spectrum of 600–633 nm. This therefore illustrates that both the simulation model and the experimental process are reasonable. This novel method has potential applications in high-accuracy calibration in the wide spectrum using correlated photons.

OCIS codes: 190.4410, 120.3940, 300.6410, 040.5250.
doi: 10.3788/COL201513.113001.

The interest in applying spontaneous parametric down-conversion (SPDC)[1] to infrared calibration in radiometry has grown significantly in recent years due to the very appealing properties of the radiation produced[2,3]. Compared with the classic calibration scheme[4], which is limited to a long transfer chain without any absolute radiometric reference, the advantages of SPDC have been becoming a matter of interest for more and more scientists. However, most of the calibration procedures described above by using the SPDC method pay little attention to the spectral characteristics, and there is still no in-depth discussion on the characteristics of the output spectrum. The spectral properties of SPDC photon pairs are especially important for optical system design and correlated photons detecting.

Several works were demonstrated for spectral characteristics based on periodically poled crystals have been published. Chen *et al.*[5] used a 532 nm laser-pumped PPKTP crystal to analyze the signal's spectral range at different temperature levels by using tunable filters without a detailed theoretical explanation. Haidar *et al.*[6,7] presented a broadband spectrum by means of a PPLN crystal pumped by a Nd:YAG laser, they discuss the influence of incident angle on spectral properties and phase mismatching, but the relationship between the crystal periodic modulation function and the incidence angle were not included. Hongjun *et al.*[8,9] expanded the wave-vector mismatch in a Taylor series and retained second order terms. Considering the limitation of the model created by Hongjun *et al.*, such as the plane wave approximation and the lack of deductions about the relationship between the crystal periodic modulation function and the incidence angle, the simulation results do not match the experimental ones. Fejer *et al.*[10] considered the relationship between the crystal periodic modulation function and the incidence angle; however, no in-depth analysis on the output spectrum of the above issue is presented.

In order to solve the limitations of the theoretical models above, our theoretical model will be divided into three parts. Firstly, the relationship between the crystal periodic modulation function and the incidence angle was obtained based on the analysis of three-wave-vector phase matching in a PPLN crystal. Then, a general mathematical model for evaluating the spectral range was developed, which analyzed the effect of the angle propagation of the pump beam and non-collinear angle on the output spectral range. With the crystal size as the range constraint, we carried out a numerical simulation with a loop algorithm and obtained the spectral range according to our model. Finally, the spectrum curve shape was determined by a discrete Fourier transform on the Gaussian-shaped pump beam and integrating it with each individual plane-wave parametric down-conversion.

An experiment was carried out to the results were compared with the theoretical predication that the simulation value and the experimental value shared a good consistency with the same spectral range and curve shape, which therefore illustrated that both the simulation model and the experimental process were reasonable and reliable.

Quasi-phase matching (QPM) was obtained by a repeated inversion of the relative phase between the forced and free waves after an odd number of coherence lengths. When these relationships were satisfied exactly[10,11], this process was described as ideal phase matching. Otherwise, the interaction may still occur with a lower efficiency of interaction. The parametric down-conversion efficiency was strongly dependent on the wave-vector mismatch, which for the first-order QPM collinear process was as[3,4]

$$\Delta k = k_p - k_s - k_i - 2\pi/\Lambda, \tag{1}$$

where $\boldsymbol{k}_l$ $(l = p, s, i)$ are the wavelength and wave vector, respectively. Λ represents the period of the modulated structure. When Δk was defined by the equation in a perfect phase-matching case, the period of non-linear crystal could thus be represented as

$$\Lambda_0 = 2\pi/(k_p - k_s - k). \tag{2}$$

As the QPM was carried out in a birefringent crystal, both the QPM effects and birefringence could occur simultaneously. The QPM condition depended on the angle between the grating vector $\boldsymbol{k}$ and the wave vector of the pump beam[7]. The implications of the QPM effects were similar to those of the angular dependence of the extraordinary index of refraction. The geometry indicated in the wave diagram is shown in Fig. 1; it takes the nonlinear case into consideration.

In Fig. 1, θ and ψ are the non-linear angles of the period structure of the wave vector $\boldsymbol{k}$ and the pump vector to the $\mathbf{Z}$ axis, respectively; hence the structure of the wave vector $\boldsymbol{k}$ can be calculated from Fig. 1, and the law of sines is expressed as[12]

$$k_p \sin\psi = k \sin\theta. \tag{3}$$

We have to point out that here we only considered the positive spatial frequency component of the grating $\boldsymbol{k}$; the negative frequency component $-\boldsymbol{k}$ was neglected. In general, this neglect was justified, because $-\boldsymbol{k}$ would be far from phase matched.

The momentum conservation (or phase matching) in the horizontal direction could be represented as

$$k_p \cos\psi = k_s + k_i + k\cos\theta. \tag{4}$$

Combining the above Eqs. (3) and (4), the period required for QPM at angle θ can be found by using the law cosines, as

$$\Lambda = \frac{2\pi}{\sqrt{k_p^2 - (k_s + k_i)^2 \sin^2\theta} - (k_s + k_i)\cos\theta}. \tag{5}$$

For $\theta = 0°$, Eq. (5) thus was simplified as $\Lambda = \Lambda_0$, which was in agreement with our previous results. Depending on the results of Eq. (5), the output spectral range could be obtained by taking account of the phase-matching condition and plane wave approximation at different incidence angles of the pump beam.

Assuming the signal vector and idler vector are collinear with the grating vector and plane wave approximation, the angle between the pump vector k_p and the surface normal is ψ. A general three-wave interaction is illustrated in Fig. 2, where α and ψ are the non-collinear angles that signal and the pump were to the $\mathbf{Z}$ axis.

Based on the results of Eq. (5), we could draw the conclusion that the period structure is greatly bound up with the angle θ. When the pump beam is incident into the crystal within a small angle and the output correlation photons are kept collinear, the wavelength of the signal depends on the value of θ. Finally, the output signal spectral range would be broadened in a certain direction. According to the above conditions, we could obtain the relationship between the spectral range of the signal channel and the angle θ.

Basically, the signal and idler photons satisfied the conditions of energy conservation and momentum conservation in the horizontal direction. This process met the conditions of

$$1/\lambda_p = 1/\lambda_s + 1/\lambda_i, \tag{6}$$

$$(k_s + k_i)\cos\alpha + k\cos\theta - k_p\cos\psi = \Delta k, \tag{7}$$

where $k_j = 2\pi n_j/\lambda_j$ $(j = p, s, i)$, and the conversion efficiency was maximum when Δk equaled 0 and decreased rapidly with the increasing wave-vector mismatch when Δk did not equal 0. One criterion for the maximum allowable wave-vector mismatching was given by $\Delta K \le 2.783/L$[13]. Substituting $\Delta K = 2.783/L$ into Eq. (7), the formula could be represented as

$$(k_s + k_i)\cos\alpha + k\cos\theta - k_{p1}\cos\psi \le 2.783/L. \tag{8}$$

where L represents the length of the PPLN crystal. In order to ensure that the pump light completely passed through the crystal, we need to give some conditions to restrict the angle of (ψ, α). According to the crystal limitation and neglected negative direction, the angle of (ψ, α) ranges

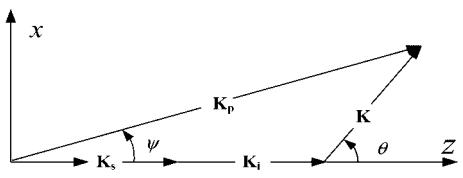

Fig. 1. Periodic modulation function vector $\boldsymbol{K}$ versus the angle θ.

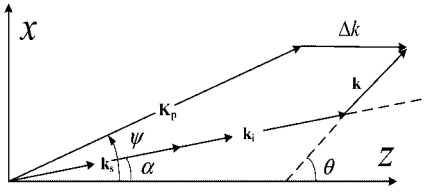

Fig. 2. Schematic diagram of the output angle of the signal light.

from 0° to 1.15°. If the above conditions could not be achieved, the correlated photons would cross through the side of the crystal.

The wavelength of the signal relates to (ψ, α, θ), based on Eq. (8). As there were three unknown variables (ψ, α, θ) and two equations, Eqs. (6) and (8), we could assign different values to the angle (ψ, α) and search for the maximum and minimum wavelength by using a loop algorithm with θ ranging from 0° to 90° by 1° steps. Finally, by subtracting the minimum values, the spectral range could be summarized as

$$\Delta\lambda_2 = \max(\lambda_s) - \min(\lambda_s). \tag{9}$$

Based on these results, we could obtain the relationship between the spectral range and the angle of the pump beam. By constraining the angle of the pump to a constant, the variation of the spectral range versus the emitting direction of the signal could be attained. Both relationships are shown in Fig. 3.

Figure 3(a) shows the variation of the spectral range of the PPLN versus the angle of the pump. From Fig. 3(a), it can be clearly observed that spectral range increased slowly from 31 nm at ψ from 0° to 35 nm when ψ equaled 1.15°. The spectral range of the signal shows a positive correlation to the angle of the pump. Figure 3(b) illustrates the dependence of the spectral range on the non-linear angle α under

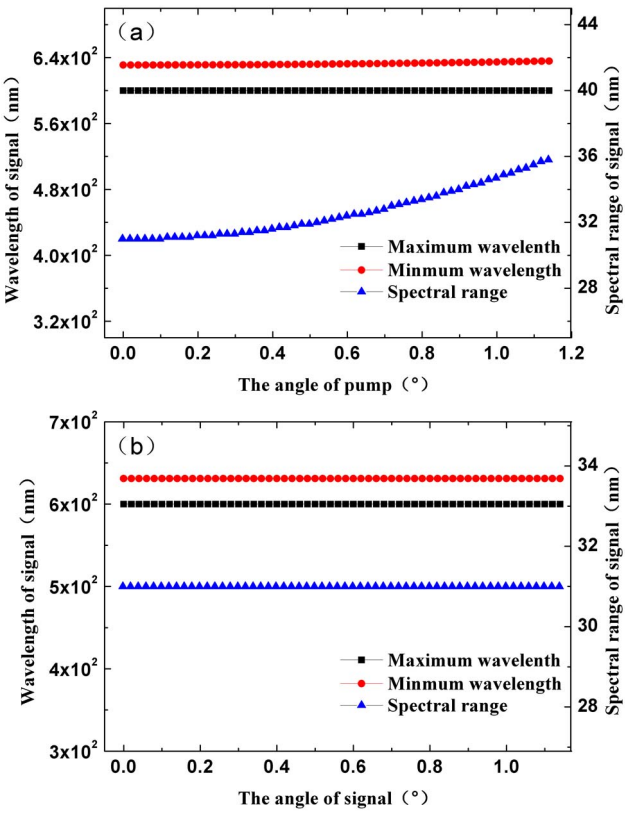

Fig. 3. Spectral range of signal channel (a) when $\alpha = 0$ the relationship between the incidence angle and the spectral range of the signal channel and (b) when $\psi = 0$, the relationship between the non-collinear angle in the crystal and the spectral range of the signal channel.

the non-collinear geometry $(\psi = 0)$ condition. From Fig. 3(b), it is apparent that the spectral range remained flat in the plot for the non-collinear angle from 0° to 1.15° and the spectral range was about 31 nm in this case. To summarize, the maximum spectral range was from 600 to 635 nm when the pump beam was not an ideal plane wave.

In the actual experiments the pump laser was not an ideal plane wave, but it could be reasonably represented by a Gaussian distribution. It has a certain divergence angle, and the existing spectrum curve of non-linear crystal would change in accordance with the pump going in different directions. These problems can be solved by carrying out a discrete Fourier transform of the pump beam. The pump beam can be considered as a series of overlapping individual planes. Each plane wave could independently generate correlated photons in accordance with the scheme in Fig. 4. Finally, the spectrum curve shape was determined by integrating the parametric down-conversion dependence of the wave-vector mismatch with each individual plane-wave.

Here, the angles α and ψ are the non-collinear angles to the **Z** axis. We assume that the signal vector and idler vector are collinear.

The pump was described as a superposition of the individual plane and monochromatic waves with a random phase, and whose power could be expressed as[12]

$$P(\omega_p, \psi, \xi) = \sum S(\omega_p) S(\psi, \xi) P_0, \tag{10}$$

where functions $S(\omega_p)$ and $S(\psi, \xi)$ denote the spectral density in the frequency and space domains, respectively. P_0 is the total pump power. Due to the narrow linewidth characteristics of the pump beam, the effects of the pump beam bandwidth can be ignored. So $S(\omega_p)$ is supposed to be a constant.

The power $\mathrm{d}p_s$ of the fluorescence signal emitted by a non-linear medium in a spectral interval $\mathrm{d}\lambda_s$ integrated over the whole solid angle[14] can be obtained using

$$P_s = \int_{\lambda_{s1}}^{\lambda_{s2}} \beta L^2 \mathrm{d}\lambda_s \int_0^{\infty} \mathrm{d}\omega_p \int_0^{2\pi} S(\omega_P) P_0 \mathrm{d}\xi \times \int_{\theta_1}^{\theta_2} S(\psi, \xi) \mathrm{sinc}^2\left(\frac{\Delta k L}{2}\right) \mathrm{d}\psi. \tag{11}$$

where ψ and ξ are the relevant angles within the non-linear crystal, and β is the non-linear coupling coefficient, which is expressed as[15]

$$\beta = (2\pi)^4 \frac{2\hbar c d_{\mathrm{eff}}^2 \lambda_p}{\varepsilon_0 n_p^2} \frac{1}{\lambda_s^5 \left(\frac{1}{\lambda_p} - \frac{1}{\lambda_s}\right)^{-2}} \int_0^L P_p(l) \mathrm{d}l \mathrm{d}\lambda. \tag{12}$$

where d_{eff} is the effective nonlinearity of the PPLN medium, and n and λ denote the index of refraction and the wavelengths, respectively. Δk is the phase mismatch, which can be defined as

$$\Delta k = k_{wp} \cos(\psi - \alpha) - k \cos(\theta - \alpha) - (k_s + k_i). \tag{13}$$

The integration over the pump power takes into account the absorption of the PPLN at 532 nm. For $P_p(l)$,

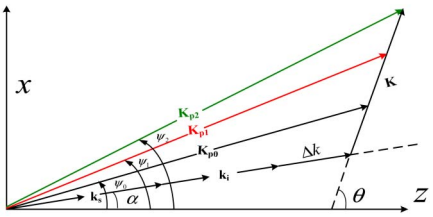

Fig. 4. Schematic diagram of the output angle of signal light based on the Fourier transform of the pump beam.

we assume Beer's law, $P_p(l) = P_P(0)e^{-\partial l}$ and the coefficient ∂ was measured using the work of Ref. [16]. The relevant parametrics of the non-linear crystals were taken from Ref. [17], and the photon flux could be can be expressed as

$$N_{\lambda}^{\mathrm{SC}}(\lambda) = \frac{\lambda}{hc} P_S. \tag{14}$$

Finally, by combining Eqs. (5) and (10)–(14), we can obtain the photon flux versus the wavelength of the signal. To demonstrate the validity and rationality of the model, an experiment should be carried out to certify the model.

The experimental setup is schematically depicted in Fig. 5. The whole setup was assembled in a single black box and consisted of three compartments, each isolated by an aperture. The pump source, with beam collimation, height adjustment, polarization, polarization rotation, and beam shape, was assembled in the first section. A 532 nm CW laser (coherent Verdi-v18, Linewidth <5 MHz), which had a maximum power of about 18 W emitting a total of 100 mW in our experiment, served as the pump source. The pump beam was first through directed two highly reflective mirrors, and then it was sent into two apertures in order to eliminate the marginal rays. Then, it was collimated into a folded mirror, which was used for height adjustment. After passing through the folded mirror, the beam was introduced into another optical bench. A Glan–Taylor prism was mounted on a rotating stage to linearly polarize the pump laser source. A half-wave plate controlled the pump polarization to measure the background noise. Lens L1 ($f = 120$ mm) was used to shape the pump beam and couple the pump beam into the PPLN crystal completely.

The second compartment consisted of the PPLN non-linear crystal, which served as the generator of the parametric fluorescence. The PPLN (50 mm × 3 mm × 1.5 mm) non-linear crystal's temperature, which was controlled by using a thermo-electric cooler with 0.1°C stability, was set to 25°C. The period of the PPLN crystal was 10.6258 μm (532 → 631 nm + 3.39 μm, collinear).

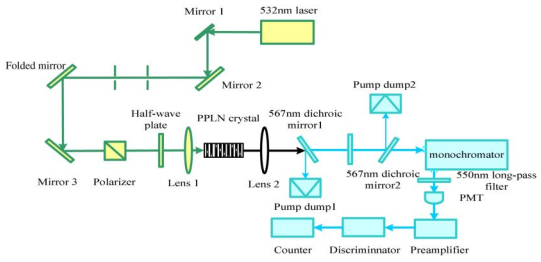

Fig. 5. Schematic diagram of broad spectrum measurements based on monochromatic scanning system.

The third compartment was the detection system, which was created by means of a photomultiplier (PMT) detector. The parametric fluorescence was collected through a composite lens, L2 ($f = 60$ mm), which formed an angular distribution pattern on the plane of the exit slit. The short-wave cutoff was set by combining two dichroic mirrors (567 nm) and a long-pass filter (550 nm), while the long-wave (infrared band) cutoff was imposed by the natural absorption limit of the PMT detector. The signal photons were separated from the pump beam by two dichroic mirrors. By controlling the dispersion of the monochromator (Zolix Omni-λ3005), the desired quasi-Lambertian correlated photon source was provided. In order to decrease background radiation of the pump, the dichroic mirrors were placed at an angle of 45°. This plan could prevent the pump from reflecting between the back and the front, which would increase the transmittance of the pump.

In order to ensure the complete pump beam coupling into the PPLN crystal, it was necessary to measure the beam spot by means of a laser beam profiler. Based on the size constraints of the PPLN crystal, the diameter of pump beam must be less than 1.5 mm. We used a telephoto lens to couple the pump beam into the crystal. The laser spot is shown in Fig. 6.

This spot diameter was about 0.5 mm, which was much smaller than the height of crystal (1.5 mm); it could be considered to meet the requirements of the experiment.

The spectral properties were measured at a scanning step of 1 nm ranging from 600 to 640 nm by using monochromatic-based facility (line-width 1 nm). The PPLN non-linear crystal's temperature was set to 25°C. Because we used only one counter in our experiment, the counts of the signals would be achieved by using a cross-measuring technique. The curve of counts rate, including background counts and signal-to-noise ratio (SNR), is shown in Fig. 7.

As we can see from Fig. 7, the output spectral range of signals from 600 to 633 nm meets the SNR requirement. When the wavelength was not in the above range, its SNR would be less than 20. The SNRs of 600 and 633 nm were 54 and 32, respectively. The position of the maximum SNR stayed at 631 nm. Compared to the theoretical value, the experimental ones were slightly smaller than 1 nm in the longer wavelengths, which probably was the result

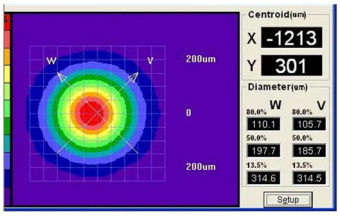

Fig. 6. Analysis of laser spot.

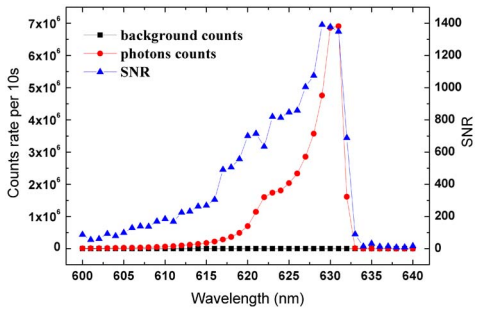

Fig. 7. Relationship between the wavelength and photon count rate.

of the complex interaction between the pump beam and the PPLN crystal when the pump was not an ideal plane wave. Because of the Gaussian distribution of the pump beam, its intensity would decrease when the exit angle increased. This would lead the rate of count to be low when the signal wavelength was far away from the center wavelength. Finally, the output waveform would become a peak shape curve whose value would increase when its wavelength was gradually closed to 631 nm

Figure 8 plots the number of detected photons and calculated spectral flux of parametric fluorescence in the PPLN crystal. The plots suggest that the simulation value and the experimental value shared a good consistency with the same spectral range and curve shape. From Fig. 8, it can be clearly observed that both profiles first increase slowly to the peak and then decline sharply, and that both curves have asymmetrical characteristics. The differences were that the slopes of curves were not the same, and the experimental curve was relatively smooth. The reason for the discrepancy was that the divergence of the pump beam will increase by exploiting the lens to focus it, and the intensity distribution would be changed in the PPLN crystal. The above processes produced an influence on the conversion of different signal wavelengths. Finally, the output curve will become smooth and the phenomenon of wavelength drift will occur. These results show that a narrow linewidth

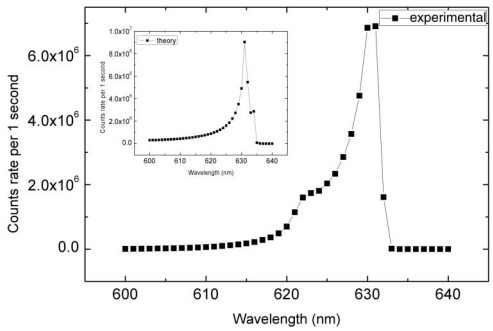

Fig. 8. Theoretical and experimental diagrams of photon count rate versus signal wavelength. The big block diagram represents the experimental data. The small diagram represents the theoretical data $(0° \le \psi \le 1.1°, \alpha = 0°, 0° \le \theta \le 90°$, Gaussian distribution of pump beam).

spectrum can be obtained by improving the pump beam quality and reducing the divergence of the pump beam.

The spectral prosperities of entangled photon pairs generated via QPM generated using parametric down-conversion is proposed and demonstrated experimentally. A general mathematical model for evaluating the spectral properties is developed with spectrum curve shape and the spectral properties. The model takes into account the effects of departures from ideal quasi-phase matching in periodicity, angle propagation, and the relationship between the crystal periodic modulation function and incidence angle. The spectrum curve shape is determined by carrying out a discrete Fourier transform on the Gaussian pump beam and integrating it with each individual plane-wave parametric down-conversion. By means of a PPLN non-linear crystal and the dispersion of monochromatic light, an experiment is carried out to certify the theory. The results show that the simulation value and the experimental value share good consistency and have the same spectral range and spectrum curve shape, which therefore illustrates that both the simulation model and the experimental process are reasonable. This novel method shows great significance for the high-accuracy calibration of the wavelengths of correlated photons.

This work was supported by the National 863 Program of China (No. 2015AA123702), the National Natural Science Foundations of China (Nos. 11204318 and 61275173), and the National Defense Science and Technology Foundation (No. J2920130004).

References

1. M. Zheng, L. Chen, X. Cai, and G. Jin, Chin. Opt. Lett. **11**, 071901 (2013).
2. S. Castelletto, I. P. Degiovanni, V. Schettini, and A. Migdal, Metrology **43**, S56 (2006).
3. S. Odate, A. Yoshizawa, D. Fukuda, and H. Tsuchida, Opt. Lett. **32**, 3176 (2007).
4. Z. Xiaobing, W. Haoyu, Z. Junping, L. Yuchen, Z. Wei, W. Leyi, and Q. Yanli, Chin. Sci. Bull. **45**, 2009 (2000).
5. J. Chen, A. J. Pearlaman, A. Ling, J. Fan, and A. Migdall, Proc. SPIE **7465**, 74650L (2012).
6. S. Haidar, T. Usami, and J. Shikata, Opt. Eng. **42**, 143 (2003).
7. C. Wei and C. C. Yang, Opt. Lett. **26**, 14129 (2001).
8. L. Hongjun, Z. Wei, C. Guofu, W. Yishan, C. Zhao, and R. Chi, App. Phys. B **79**, 569 (2004).
9. N. P. Barnes and V. J. Corcoran, Appl. Opt. **15**, 696 (1976).
10. M. M. Fejer, G. A. Magel, D. H. Jundt, and R. L. Byer, IEEE **28**, 2631 (1992).
11. D. Zhong, Chin. Opt. Lett. **12**, S11901 (2014).
12. S. Prabhakar, S. G. Reeddy, A. Aadhi, A. Kumar, P. Chirthrabhanu, G. K. Samanta, and R. P. Singh, Opt. Commun. **326**, 64 (2014).
13. Y. Chen, X. Chen, Y. Xia, X. Zeng, and Y. Chen, Proc. SPIE **4581**, 402 (2001)
14. G. Tamošauskas, J. Galinis, A. Dubietis, and A. Piskarskas, Opt. Express **18**, 4310 (2010).
15. G. Brida, M. Genovese, and C. Novero, Eur. Phys. J. D **8**, 273 (2000).
16. P. Kumbhakar and T. Kobayashi, Appl. Phys. B **78**, 165 (2004).
17. D. Jundt, Opt. Lett. **22**, 1553 (1977).